Geomechanics and Engineering, *Vol. 27, No. 6 (2021) 537-550*
https://doi.org/10.12989/gae.2021.27.6.537

Research on no coal pillar protection technology in a double lane with pre-set isolation wall

Hui Liu[1,3,4], Xuelong Li*[2,5,6], Xin Gao[5], Kun Long[6] and Peng Chen[7]

[1]*Key Laboratory of Gas and Fire Control for Coal Mines, Ministry of Education, China University of Mining and Technology, Xuzhou 221116, Jiangsu, China*
[2]*Mine Disaster Prevention and Control-Ministry of State Key Laboratory Breeding Base, Shandong University of Science and Technology, Qingdao, 266590, China*
[3]*Gucheng Coal Mine, Shandong Energy Lining Coal Mine Group, Jining, 272100, Shandong, China*
[4]*School of Safety Engineering, China University of Mining and Technology, Xuzhou 221116, Jiangsu, China*
[5]*College of Energy and Mining Engineering, Shandong University of Science and Technology, Qingdao 266590, China*
[6]*State Key Laboratory of Coal Mine Disaster Dynamics and Control, College of Resource and Safety Engineering, Chongqing University, Chongqing 400030, China*
[7]*School of Safety Engineering, North China Institute of Science & Technology, Langfang 101601, China*

(*Received November 24, 2020, Revised October 22, 2021, Accepted November 10, 2021*)

Abstract. There are various technical problems need to be solved in the construction process of pre-setting an isolation wall into a double lane in the outburst prone mine. This study presents a methodology that pre-setting an isolation wall into a double lane without a coal pillar. This requires the excavation of two small section roadways to dig a wide section roadway, followed by construction of the separation wall. During this process the connecting lane is reserved. In order to ensure the stability of the separation wall, the required bearing capacity of the isolation wall is 4.66 MN/m and the deformation of the isolation wall is approximately 25 cm. To reduce the difficulty of implementing support the roadway is driven by 5 m/d. After the construction of the separation wall, the left side coal wall is brushed 1.5 m to make the width of the gas roadway reach 2.5 m and the roadway support utilizes anchor rod, ladder beam, anchor cable beam and net configuration. During construction, the concrete pump and removable self-propelled hydraulic wall mold are used to pump and pour the concrete of the isolation wall. In the process of mining, the stress distribution of coal body and isolation wall is detected and measured on site. The results demonstrate that the deformation of the surrounding rock of roadway and separation of roof in the roadway is small. The stress of the bolt and anchor cable is within equipment tolerance validating their selection. The roadway is well supported and the intended goal is achieved. The methodology can be used for reference for similar mine gas control.

Keywords: double lane with pre-set isolation wall; high gas mine; mining monitor; roadway protection without coal pillar

1. Introduction

Coal is the primary energy source in China, and the coal industry plays an important role in the broader Chinese economy. Coal accounted for 77% of national energy production and 70% of consumption, this pattern will not change in the coming decades (Feng *et al.* 2020). Dependent on various geographic factors, the coal occurrence is relatively complex, and the majority of mines utilize underground mining techniques. Roadways are the key structures associated with coal mine production, and excavation and maintenance costs are quite large (Bai *et al.* 2016, Brunschwiler *et al.* 2013, Hu *et al.* 2019). Chinese coal mines are reported to dig approximately 13000 Km of new roadways every year, of which about 80% are affected by mining activities (Li *et al.* 2021, Li *et al.* 2021). Traditionally, the favored method to control coal mine pressure and prevent damage to roadways is to retain the coal pillars. Typically, a placement of coal pillars every 10~30 meters ensures protection of the roadway (Hu *et al.* 2019, Vladimir *et al.* 2017). Although this method allows for improved safety and less maintenance of the roadway, there are some problems in retaining roadway pillars, such as (Najafi *et al.* 2011, Lobanova *et al.* 2017, Yan e*t al.* 2018, Kong *et al.* 2020): (1) It could increase the coal loss and reducing the recovery rate. (2) The method is not conducive to preventing and controlling rock bursts, spontaneous combustion of coal and other mine disasters; (3) Wide coal pillars can cause stress in the surrounding formations, affecting the mining of adjacent coal seams and the stability of roadway floor.

Non pillar roadway protection involves arranging the roadway such that the edge of coal body and the junction of the goaf meet (Qin *et al.* 2016, Zhu *et al.* 2020). Compared with traditional coal pillar roadway retention, the protection pillar located between the upper and lower sections is removed, improving the mine recovery of coal and offering benefits to mine safety. There are two main types of roadway protection without utilizing coal pillars: (1)

*Corresponding author, Dr.
E-mail: lixlcumt@126.com

ISSN: 2005-307X (Print), 2092-6219 (Online)

Driving along the goaf or (2) Retaining the roadway along the goaf. In order to achieve minimal roadway excavation, which in turn increases mine economics, several major coal producing countries worldwide adopt a reciprocating "Z" mining method (Song 2015, David *et al*. 2015). This entails a forward and backward gob side entry retaining technique and small coal pillar driving along the goaf. In order to develop and improve non pillar mining, a large number of studies have been carried out on strata pressure behavior, applicable conditions, support forms and new support materials (Wu *et al.* 2020, Wang *et al.* 2020). In the late 1970s, it began to be widely publicized and used across different mines. In the 1980s, a large number of theoretical, field and laboratory studies were carried out investigating the ground pressure law, theory of stress distribution in coal bodies adjacent to goaf, and the "support mechanism". When utilizing non pillar roadway protection, support rocks have become the main means of roadway support, promoting the development of the technology (Wang *et al.* 2015, Tiskumara *et al.* 2015, Cheng *et al.* 2020, Zhang *et al.* 2021). In China, gob side entry driving is often used, as well as to a lesser extent, side entry retaining.

Problems associated with gob side entry driving mainly focus on whether to set up small coal pillars, their size, optimal driving time and distance from the goaf. As small coal pillars are easily fractured and during ventilation can naturally ignite, they should not be left in the roadway (Guo *et al.* 2016, Wang *et al.* 2019, Zhang *et al.* 2020). However, consider coal pillars can prevent mining of gangue and ponding, pillars are generally used in practice. In recent years, some mines have used the preset filling belt instead of the small coal pillar to drive along the goaf (Singh *et al.* 2011, Wohlford *et al.* 2019, Shen *et al.* 2019). That is, the section of coal pillar between the upper and lower working faces is replaced by the preset filling belt, and the lower section of roadway is driven along. This technology overcomes the disadvantages of traditional narrow coal pillars for roadway protection or fully driving along the goaf, improving coal resource recovery (Yang *et al.* 2019).

With respect to gob side entry retaining, studies are primarily theoretical analyses, including the selection of support materials, isolation of goaf and roadway support. Although now utilized less, traditional methods of roadway retention have the disadvantages of low support strength and large roadway deformation. Presently, artificial blocks and rigid filling belts are widely used, and the latter is subdivided into use of high water quick setting material, ordinary concrete, early strength concrete, anhydrite, etc (Wang *et al.* 2011, Tinnea *et al.* 2016, Zhang *et al.* 2019). During their investigations, He *et al*. (Zhu *et al.* 2020) put forward a method of pressure relief and roof cutting along goaf to form a roadway without coal pillars in a deep mine working face. During this technique the roof of the gob side roadway is cracked in advance, and the connection between gob side roadway roof, direct roof and basic roof are cut off. Under the weight pressure, the stope roof will be cut off along the presplit face to form the roadway side, isolating the goaf and supporting the upper strata.

Due to increases of yield and mining intensity at the working face, gas emissions can increase rapidly. U-type ventilation systems cannot effectively control large levels of gas release at the working face, so special gas drainage roadways should be considered during mine planning (Soares and Cherneva 2005, Chen *et al.* 2018, Sander and Connell 2012). Setting a gas roadway can transform the original U-type ventilation system into a "U + L" ventilation system, which effectively solves the problem of large volume gas release at the upper corner of the working face. However, there are few studies that investigate the problems of utilizing gas roadways, such as roadway deformation, maintaining support and retention of roadway pillars. There are two primary considerations when designing the size of coal pillars during gas roadway protection (Singh *et al.* 2011, Rezaei *et al.* 2015, Wang *et al.* 2019, Zou *et al.* 2020): (1) The size of the pillar between the gas roadway and upper section, and (2) the size of the coal pillar between gas roadway and return air roadway. Analysis of the deformation mechanism and support measures of the gas roadway is not sufficient, the influence of double lane driving on the roof structure and surrounding rock stress distribution is not considered during these calculations.

This paper research on the technology of protecting a roadway without using coal pillars in an outburst prone mine using a modified gas roadway. In view of the technical requirements and problems to be solved during construction, this paper presents a scheme of pre-setting an isolation wall into a double lane without coal pillar. To enable this, the mechanical model of the roof plate of the double lane was established for mechanical analysis, the bearing capacity and reasonable width of the prefabricated isolation wall were calculated, and a field test was conducted in 9106 lane of Anshun coal mine, through monitoring the deformation of the surrounding rock, the roof plate leaving the layer, the anchor rod (rope) force, the isolation wall force, etc. The overall support effect of the roadway is good, the force on the isolation wall is small, the strength meets the requirements and the expected target is achieved.

2 Working face overview and problems description

2.1 Overview of mine and working face

Anshun mine, located in the Dadongkou minefield, is 14km north of Anshun City, Guizhou Province, China. Its administrative divisions are subordinate to Jiaozishan Town, Anshun City, Wozi Township and Maodong Township, Baiyan District, Puding County. The geographical coordinates of the mine are: 105°50′37.5″ ~ 105°56′15″ E, 26°20′00″ ~ 26°23′45″ N.

Transportation to the mine field is serviced by rail. There is a special line (standard gauge railway) servicing Anshun coal mine to Anshun city. The total length of the special line is 20.4 Km, which is industrial enterprise standard. The main line of Yunnan Guizhou highway passes through Anshun, and there is approximately 16 Km of asphalt pavement road from the coal mine to Anshun. The location of the mine field is shown in Fig. 1.

Fig. 1 Locations of Anshun Coal Mine

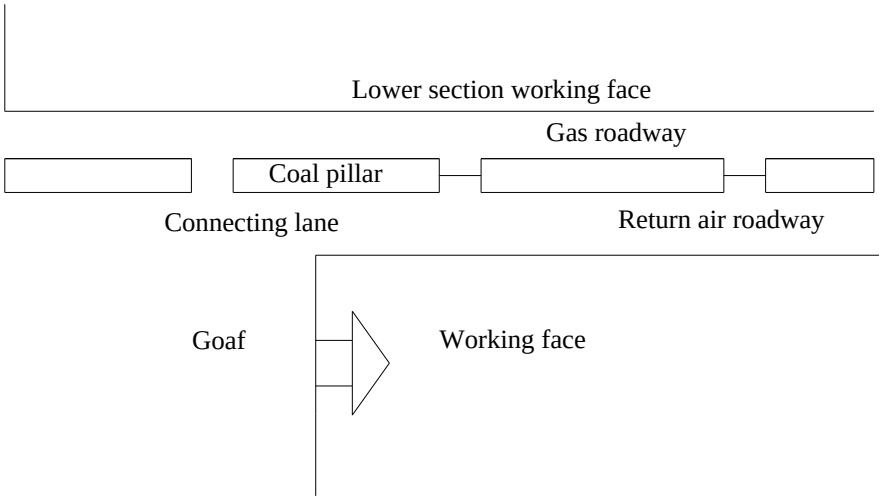

Fig. 2 Sketch map of “U+L” ventilating system with laneway

The 9106 working face is a comprehensive mechanized coal mining face. The design of the 9106 upper gateway is 673 m. The coal seam is stable and the structure is geologically simple. The thickness of the seam typically ranges from 1.4 m ~ 1.8 m, with an average thickness of 1.6 m. The coal seam dip angle varies from 2°~ 8°. The physical property of the coal seam is black and bright, which is brittle and can be easily broken. The fracture surface is uneven and glossy. The roof structure has no false roof and the direct roof consists of gray carbonaceous clay rock, with a thickness ranging from 3.3 m ~ 4.0 m, with an average thickness of 3.58 m. The basic top consists of light gray fine sandstone, with an average thickness of 3.55 m. The pseudo bottom is dark gray carbonaceous clay rock, the thickness of which ranges from 0.2 m ~ 0.5 m, having an average thickness is 0.3 m. Finally, the direct bottom is siltstone clay rock, which has a thickness of 9.1 m ~ 9.8 m, and an average thickness of 9.6 m.

2.2 Questions description

In order to investigate the problem of gas overrun in the upper corner and air return chute of the working face, a special gas drainage roadway was arranged. This required setting a 4 m protective coal pillar at the side of the air return roadway to form a "U + L" ventilation system (Fig. 2). The gas emitted from goaf and the upper No. 8 coal seam is primarily discharged by a gas lane through connecting the roadways set between isolated pillars to control gas outbursts.

To facilitate this mode of ventilation, two roadways must be excavated at the return air side before mining, one for normal return air and pedestrians, the other for gas discharge. A 4 m coal pillar is set between the two roadways, and the connecting roadway was used to connect the return air roadway and the gas roadway appropriately. This requires two independent roadways (return air and gas roadways), and consequently there are some problems when considering driving. Firstly, as the mine is a prone to gas outbursts, the phenomenon of gas overrun will often occur during driving. It needs a significant period for gas drainage, and excavation can only be continued once gas emissions meet safety regulations. The long waiting time restricts the tunneling speed. The relationship between mining and excavation is closely related. If the two roadways are driven separately this will result in conditions where the mining speed is restricted and the mine may be unable to reach the

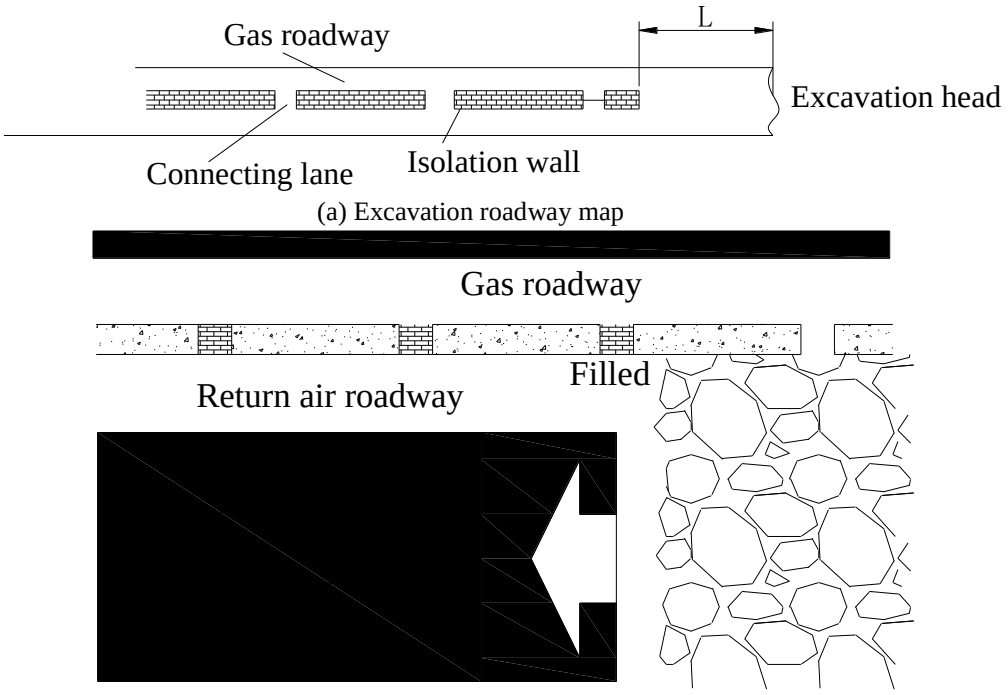

(a) Excavation roadway map

(b) Stope face map

Fig. 3 Sketch map of presetting seperation wall to make double laneways

targeted production capacity. Secondly, a 4 m wide coal pillar between the roadways reduces resource recovery whilst also has associated safety issues, such as stress concentration and potentially the spontaneous combustion of the coal pillar (Li *et al.* 2021, Liu *et al.* 2021). Thirdly, the two roadways need to lay pipes and cables separately, consuming significant manpower and resources. Fourthly, when the original gas roadway is used as a transport roadway during section mining, the roadway deformation is serious due to the small width of coal pillars between the roadways, resulting in increased repairs.

To solve these existing problems in light of the actual mine site situation, this study proposes a scheme of pre-setting the separation wall in the lane into the double roadway without a coal pillar. This requires the excavation of two small roadway sections, digging a wide cross-section roadway first, followed by then building the isolation wall between the two roadways. This will separate the roadway and reserve the connecting roadway to allow roadway protection without coal pillars (Fig. 3). When mining in the next section, the isolation wall plays a similar role as the side support of the middle lane along the goaf. This retains the gas lane and brushes the side slope in the later stage as the transportation roadway of the next section. This continues to allow protection of the roadway without coal pillars.

3 Mechanical analysis of double lane with pre-set separation wall in roadway

3.1 Mechanical model of double roadway roof

In the process of mining, the return air roadway located in the double roadway (return air and gas) is not retained. The isolation wall plays the role of supporting the side entry in the gob side retaining roadway, and the gas roadway is retained. The roof structure model under this scheme is similar, but not identical, to traditional gob side entry retaining.

The traditional method of gob-side entry retaining is to fill the goaf-side near the roadway to form a strip resulting in the roadway side support body being on the goaf-side, which is not protected by the original support (Fig. 4(a)). In comparison, the double lane method has the separation wall constructed during the process of roadway excavation, this results in the entire structure not being located in the goaf and protected by the roadway support (Fig. 4(b)). During the process of mining, with the basic roof bending and sinking, the isolation wall is located close to the goaf. To allow roadway support a part of the original roof is retained, which is different from the side cutting along the filling body of roadway side support.

Similar to the gob-side entry retaining, movement of the overlying roof strata of double roadways can also be separated into three distinct periods after the upper face is pushed. Specifically, (1) Early active period (small structure formation), (2) Transition period (large structure formation) and (3) Later active period (stable period).

(1) Early active period: Due mining of the working face, the support moves forward and the roof rock layer behind the working face loses support. This results in the direct roof on the goaf-side being cut off and a small structure is formed. This period primarily comprises of the collapse of the direct roof, filling the goaf and the subsidence of the basic roof. Roadway roof deformation is small during this process, as demonstrated in Fig. 5.

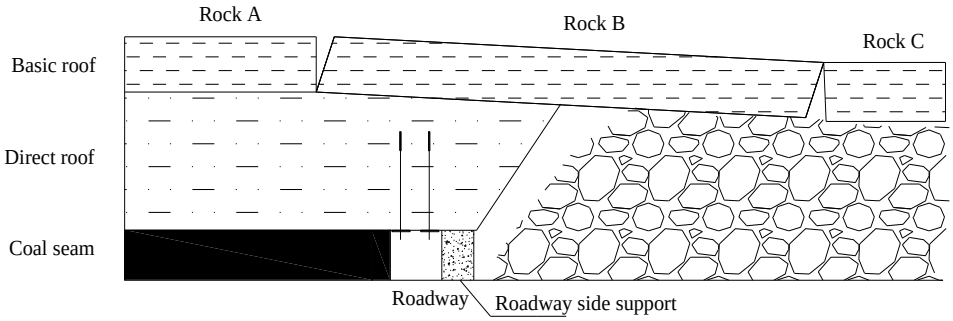

(a) Roof structure model of gob side entry retaining

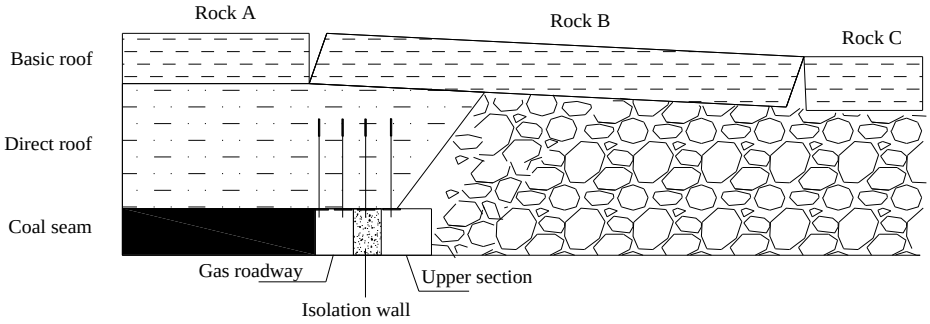

(b) Double lane roof structure model

Fig. 4 Roof structure comparison between gob-side entry retaining and double laneways

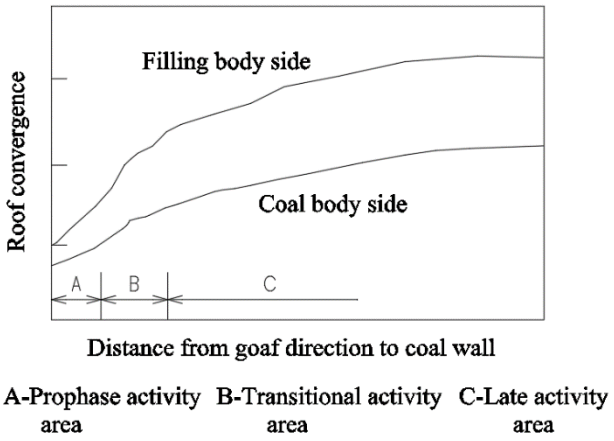

Fig. 5 Curve of roof convergence

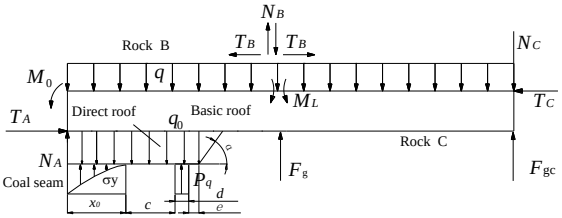

Fig. 6 Mechanical model of double laneways

(2) Transition period: With advancement of the working face, the abutment pressure of the coal body on both sides of the working face will increase. This results in the coal body appearing to have plastic failure and a large reduction in the bearing capacity. This state is extremely unstable and cannot prevent the bending settlement of the overlying strata. A significant reduction of contact stress between strata and basic top depth will act upon the coal body causing a fracture. One end of block B is supported by the coal body, and the other end is supported by gangue contained in the goaf. With this support, a large structure will be formed. During this period, the roof rotation deformation speed is fast and deformation is large. This can account for 60 ~ 70% of the total roadway deformation.

(3) Later active period: With the gradual compaction of gangue, the upper strata will also break, deform and sink, damaging the coal wall and even the direct roof, increasing the range of support pressure, moving the peak value, and the sinking the roof. In this stage, the subsidence speed of the roof is small and the deformation is minor.

Through analysis of the above periods a mechanical model of double roadway roof can be established. This is demonstrated in Fig. 6.

In order to simplify the calculations some conditions are idealized. These are described as follows:

Under the action of the isolation wall, the direct roof cuts off and fills the goaf. The cutting position is a specified distance from the isolation wall and extends upward at a defined angle. (2) The basic roof is divided by the elastic-plastic zone of the coal body and rotates towards the goaf. Block A, B and other structures are formed, in which block B is supported by the goaf and the direct roof. (3) The direct roof rotates together with the basic roof, and its rotation axis is at the junction of the elastic-plastic zone. The rotation angle of the direct roof is slightly smaller than that of the basic roof, and there is a degree of separation between them. (4) According to the beam masonry theory, the horizontal thrust between block B and block C is calculated according to the moment balance. The shear force between block B

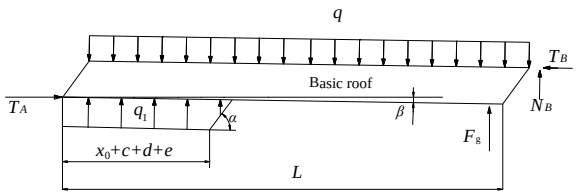

Fig. 7 Stress analysis of structure B

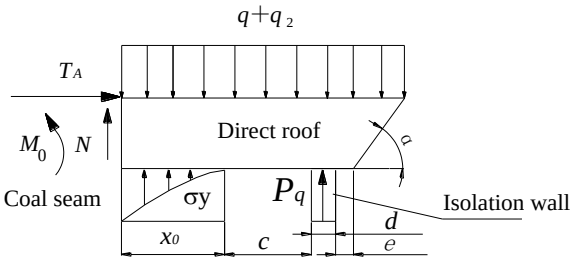

Fig. 8 Stress analysis on immediate roof

and block C is negligible and calculated as zero during analysis. (5) The results demonstrate that the force of unstable rock strata above the basic roof is uniformly loaded on the basic roof. The force from the direct roof to the basic roof is calculated according to a uniform distribution. (6) The limit equilibrium theory is used to analyse the calculation of the side support force and plastic zone of the coal body. (7) The force provided by the bolt mesh support in the roadway is smaller than that of the isolation wall, which is ignored in the calculation.

3.2 Bearing capacity and reasonable width of prefabricated partition wall

The mechanical model of basic top block B is shown in Fig. 7.

The force balance in the Y direction and moment balance in the lower left corner of block B.

$$\begin{cases} F_Y = 0 \\ M = 0 \end{cases} \tag{1}$$

If each parameter is entered then (Mcclung 2010, Zhou *et al.* 2020, Xue *et al.* 2020)

$$\begin{cases} q \times L - F_g - q_1 \times f + N_B = 0 \\ q \times L^2 / 2 - q_1 \times f^2 / 2 - T_B(h_b - \Delta S_B) - F_g \times L = 0 \\ f = x_0 + c + d + e + h_d / \tan\alpha \end{cases} \tag{2}$$

(1) Where q is the force produced by the weight of the basic roof and the soft rock above (KN/m^2), q_1 is the force of the direct roof to the basic roof (KN/m^2), F_g is the supporting force of the gangue (KN/m), h_d is the thickness of the direct roof - the span behind that can fill the goaf (m), h_b is the thickness of the basic roof (m), N_B is the shear force of Block C on Block B (KN/m), T_B is the thrust of Block C on Block B (KN/m), ΔS_B is the right end subsidence of block B during rotation and can be calculated as $\Delta S_B = L \times \sin\beta$ (m), α is the rock breaking angle, (o), β is the rotation subsidence angle of block B (o), x_0 is the width of the plastic zone generated by the section mining (m), C is the width of the gas lane (m), d is the width of isolation wall (m), e is the reserved width of the original roadway during roof cutting under the action of roadway support (m) and L is the length of block B, i.e. weighting step distance of basic top cycle (m).

(2) The width of the plastic zone is determined by measurement and can also be calculated according to the limit equilibrium theory (Li *et al*. 2021, Wang *et al.* 2020, Zhou *et al.* 2020).

(3) The width of the plastic zone is determined by measurement and can also be calculated according to the limit equilibrium theory (Li *et al*. 2021, Wang *et al.* 2020, Zhou *et al.* 2020).

$$x_0 = \frac{mA}{2\tan\Phi_0} \ln\left[\frac{K\gamma H + \frac{C_0}{\tan\Phi_0}}{\frac{C_0}{\tan\Phi_0} + \frac{P_Z}{A}}\right] \tag{3}$$

Where m is the mining height of working face (m), A is the lateral pressure coefficient, Φ_0 is the friction angle in the coal and rock mass (°), C_0 is the cohesion in the coal and rock mass (MPa), K is the stress concentration coefficient, γ is the average bulk density of overlying strata (MN/ m^3) H is the buried depth of roadway (m), P_Z is the support resistance of the upper section of the working face roadway (MPa).

The force q produced by the weight of the basic roof and the soft rock above is generally taken as the weight of 5~8 times the thickness of the basic roof. According to the masonry beam theory, the shear force N_B between block B and block C is zero, q_1 and F_g are obtained according to Eq. (3).

$$\begin{cases} q_1 = \dfrac{qL^2/2 + T_B(h_b - \Delta S_B)}{fL - f^2/2} \\ F_g = qL - \dfrac{qL^2/2 + T_B(h_b - \Delta S_B)}{L - f/2} \end{cases} \tag{4}$$

The stress of the direct roof is shown in Fig. 8, and the left boundary is the elastic-plastic interface of the coal body.

We know from the moment equilibrium.

$$(q_2 + q_0) f^2/2 - M_0 - \int_0^{x_0} \sigma_y (x_0 - x) dx - P_q(x_0 + c + d/2) = 0 \tag{5}$$

Where q_0 is the weight of the direct roof, (KN/m2), q_2 is the force of the basic to direct roof, equal to q_1, (KN/m^2), M_0 is the residual of the bending moment of the direct roof, (KN·m), P_q is the bearing capacity of the isolation wall (KN/m) and σ_y is the supporting force of the coal body in the plastic zone (KN/m). According to the limit-equilibrium analysis, it can be calculated according to Eq. (6). Calculating the required carrying capacity of the separation wall is expressed by Eq. (7).

Table 1 Width-height ratio of the backfill in some gob-side entry retaining

Test location	Ji 2 mine	Pangzhuang mine	Jingang mine	Faer mine	Zhaoguan mine
Mining height(m)	1.6	2.0	2.1	1.9	1.3
Roadway support mode	Anchor nets cables	Shield	Anchor nets cables	Anchor nets cables	Anchor nets cables
Roadside support mode	Concrete pouring	High water ash and slag casting	Concrete pouring	Concrete block	High water material casting
Backfill height (m)	2.4	2.0	2.1	2.2	1.3
Backfill width (m)	1.5	1.2	1.0	1.5	1.5
Aspect ratio	0.63	0.60	0.48	0.68	1.2

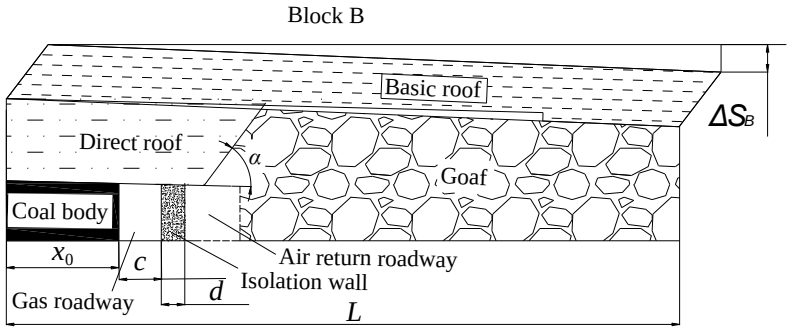

Fig. 9 Calculation model of separation wall deformation

$$\sigma_y = (\frac{C_0}{\tan\Phi_0} + \frac{P_Z}{A})e^{\frac{2\tan\Phi_0}{mA}\cdot x} - \frac{C_0}{\tan\Phi_0} \quad (6)$$

$$P_q = \frac{(q_1 + q_0) f^2 / 2 - M_0 - \int_0^{x_0} \sigma_y (x_0 - x)}{x_0 + c + d/2} \quad (7)$$

The relationship between the width and strength requirements of the separation wall can be expressed as follows

$$d = \frac{P_q}{P} \quad (8)$$

Where P is the uniaxial compressive strength of the isolation wall, KN/m^2.

During design, when considering the compressive strength of the isolation wall, its stability must be guaranteed. The primary parameter characterizing the stability is the aspect ratio, which is generally not less than 0.6. The width and height of filling body of gob side entry retaining in selected coal mines is reported in Table 1 (Pokharel 2010, Mahdi *et al.* 2020, Rezagholilou *et al.* 2015).

The height of the 9106 roadway in the Anshun coal mine is 2.0m. Considering the stability of the environment, the width of the isolation wall is 1m.

The monitoring results of ground pressure behavior near the 9100 working face, in conjunction with measurements at the working face give the following mechanical parameters: x_0= 6 m ; h_d = 3.6 m, h_b = 9 m, α = 45°, ΔS_B= 0.7 m, c = 2.5 m, d = 1.0 m ; e = 0.5 m ; L = 22 m, q = 336 KN/m^2, q_0 = 90 KN/m^2, m= 1.6 m, A= 1.3, Φ_0= 25° ; C_0= 1 MPa ; K= 3 ; γ = 25 MN/m^2 ; H= 375 m, p_z= 0.2 MPa. To ensure a safe mining environment, the residual bending moment of direct jacking is assumed to be zero.

According to the calculation, the required bearing capacity of the wall is 4.66 MN/m, and the uniaxial compressive strength of the wall is 4.66 MPa.

3.3 Separation wall compression

During the process of gob side entry retaining, fracturing and rotary subsidence of the basic roof is inevitable. The roadway side support needs to allow for specific deformation. The separation wall in the double lane plays the role of roadway side support, and its deformation is required to be analyzed. In order to simplify the analysis, it is assumed that there is no separation layer between the basic roof and the direct roof. It is also assumed that the deformation calculation model for the isolation wall is based on the structure formed by the fracture of the basic roof (Fig. 9).

According to the analysis undertaken in Section 3.1, the deformation of the isolation wall is

$$\Delta h = \frac{x_0 + c + d/2}{L} \Delta S_B \quad (9)$$

Where, Δh is the deformation of isolation wall (m). The designation of the other parameters is as per previous descriptions.

The calculation indicates that the deformation of the isolation wall is 25 cm. This deformation value is large, requiring that the isolation wall is designed appropriately to adapt to the movement of the roadway roof strata. When the material selected does not have a large deformation capacity, it is necessary to install or retrofit a suitable material with reasonable yield deformation.

4. Field test and effect evaluation

4.1 Wide section roadway support and isolation wall construction

As the roadway has a large cross-section, the gas drainage drilling field should be arranged during the driving process, increasing the width of some roadways. In order to reduce the difficulty of roadway support, the excavation is carried out as 5 m. After the construction of the separation wall is completed, the left side wall is extended by 1.5 m to ensure the width of the gas roadway reaches 2.5 m. During mining the gas roadway is retained as the transportation roadway of the next section. When the gas roadway requires repairs the left side of coal wall is extended for a second time to meet width requirements of the transportation roadway (Fig. 10).

The wide face roadway is divided into two through the construction of separation wall after 5 m of driving. These two sections comprise of a return air lane and a transport roadway. As the support strength of the gas roadway is required to be higher, bolt and anchor cables are added after side brushing. Measures such as hanging nets and increasing the support density should be utilized in sections with faults. If roof fall risks exist and bolt and anchor cable support cannot meet the safety requirements then a metal shed can be used. During the installation of anchor bolts, ladder beams and anchor cables to provide support, the mesh is hung to provide additional support. Likewise, the anchor cable support will take the form of an anchor cable beam. The anchor cable beam of the return air and gas roadways are arranged for their specific requirements.

Due to the destabilizing influence of fully mechanized excavators, bridge belt and other equipment, floating coal cleaning, isolation wall and connecting roadway construction is typically carried out approximately 50 m from the excavation head. The concrete pump is used to pour concrete with a detachable self-moving hydraulic wall mold and other peripheral equipment. The mixing device and concrete pump were placed at the gas drainage drilling site (3 m × 3 m× 2 m, with an interval of 50 m and moved forward once every 100 m.

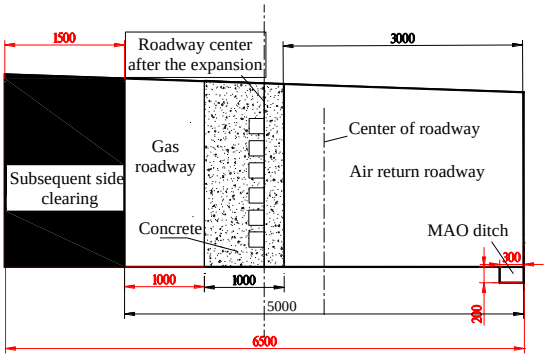

Fig. 10 Setch map of roadway section

Fig. 11 Photo of the roof-contacted filling by side of gas laneway (tunnelling direction)

In order to ensure the support of the isolation wall a space of 20 cm (determined by calculations detailed in Section 3.3) was reserved between the isolation wall and the roof. After allowing 7 days for the concrete to cure, the top was connected with square timber and bags of gangue (Fig. 11) to allow the isolation wall to relieve pressure during the mining process and prevent deformation. After confirming that the roadway is stable and compacted, the shotcrete was sealed, and its grade strength is at least C20.

A 2.5 m wide connecting lane was reserved every 25 m (weighting cycle) of the isolation wall span. The contact lane was filled with gangue bags and sealed with shotcrete. When the working face is mined to this position, the connecting roadway will be opened.

4.2 Field measurement and analysis of roadway deformation and stress characteristics

In order to verify the impact of using the separation wall to create a double lane, it is necessary to conduct on-site monitoring. A comprehensive analysis of the relevant calculation parameters allows for optimization and modification of the original technical design. During normal mine operation gas lane personnel cannot enter and monitoring is used primarily for the return air roadway. The parameters monitored include the surrounding rock deformation, roof separation, bolt

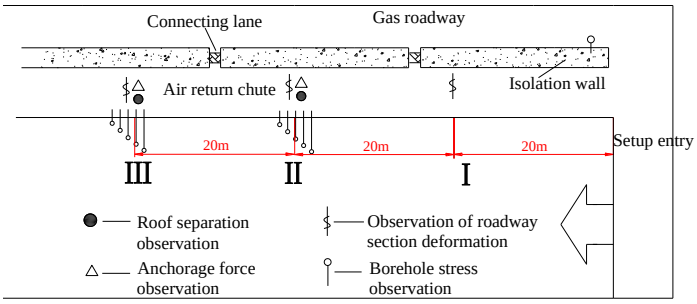

Fig. 12 Layout of station in roadway

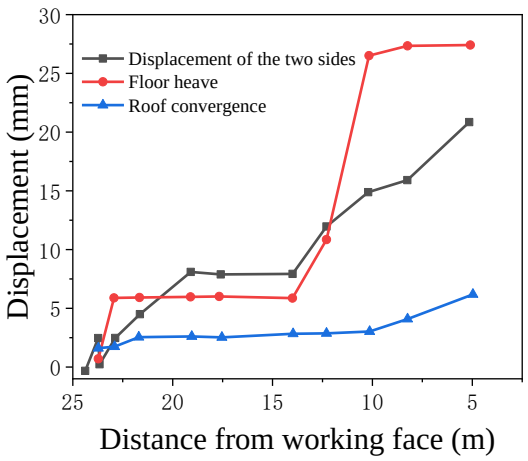

(a) Rock deformation at Section I

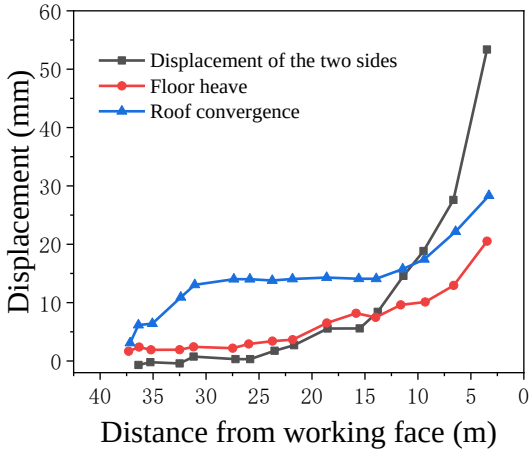

(b) Rock deformation at Section II

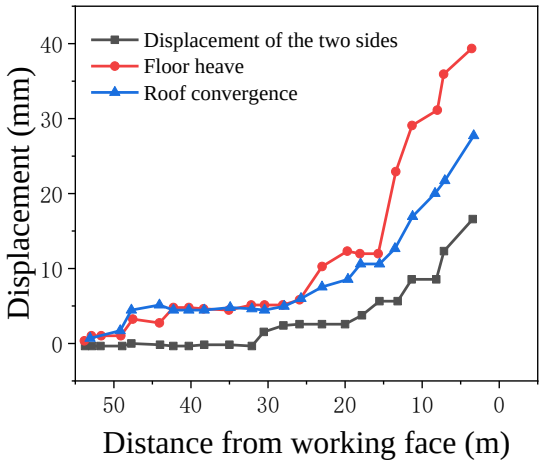

(c) Rock deformation at Section III

Fig. 13 Variation curve of surrounding rock deformation with working face advance at different sections

(cable) stress and isolation wall stress. Depending upon the required content to monitor, three measuring stations were commissioned in the return air roadway, which are approximately 20, 40 and 60 m away from the open off cut (labelled as I, II and III in Fig. 12).

4.2.1 Deformation characteristics of roadway surrounding rock

The deformation of rock surrounding the roadway is measured by cross point method. This entails setting four base points on the roof and two sides, with the roadway deformation measured by monitoring the distance change. The observation results of stations I, II and III are shown in Fig. 13 and Table 2.

In the three monitored sections, the maximum subsidence of the roof is 28 mm and the maximum deformation velocity is 3.5 mm/d. The maximum heave of the floor is 39 mm, the maximum deformation velocity 10 mm/d, the maximum displacement of two sides is 58 mm, and the maximum deformation velocity is 8.8 mm/d. The maximum influence range of the dynamic pressure of mining on the surrounding rock deformation is approximately 25 m, which is consistent with the 25 m

Table 2 Statistical table of rock deformation

Fracture surface		1#	2#	3#	Average
Roof	Maximum subsidence (mm)	6	28	28	
	Maximum speed (mm/d)	2	3.5	2.8	
	Average speed (mm/d)	0.6	1.6	1.2	
	Influence range (m)	23	Not obvious	25	24
Floor	Maximum floor heave (mm)	27	20	39	
	Maximum speed (mm/d)	10	7	5	
	Average speed (mm/d)	2.7	1.25	1.7	
	Influence range (m)	23	25	26	24.7
Department	Maximum movement (mm)	21	58	17	
	Maximum speed (mm/d)	5	8.8	4	
	Average speed (mm/d)	1.9	3.3	0.7	
	Influence range (m)	23	25	30	26

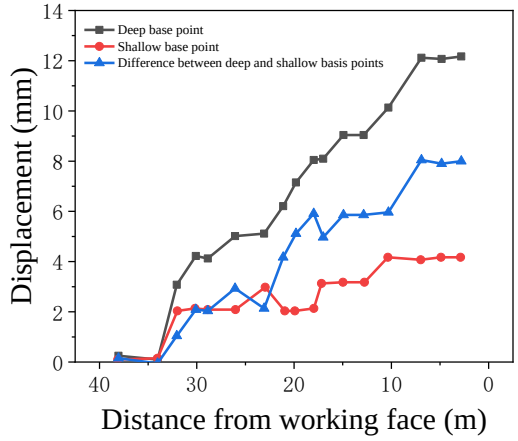

Fig. 14 Curve of roof bedding separation at measuring point 1#

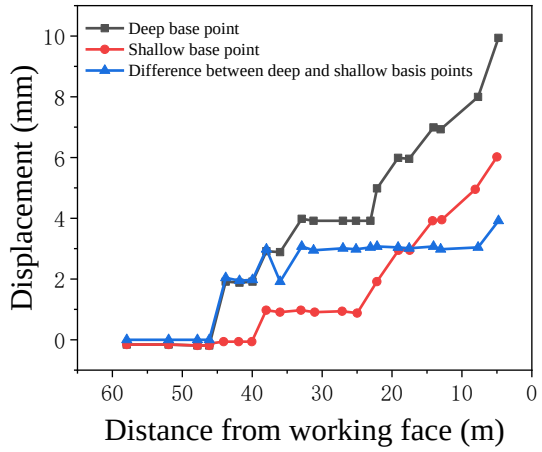

Fig. 15 Curve of roof bedding separation at measuring point 2#

advance support distance. Once the deformation speed enters the range of 10-15 m and acceleration is measured, and should be located in the stress concentration area of the advance support in front of the coal wall.

Generally, the displacement of the two sides is smaller than the subsidence of the roof, and the deformation speed is also smaller than the other two types of deformation. The floor heave of three sections is expected, but generally, when the floor heave is greater than 200 mm, it will affect underground transportation and ventilation. During this study the maximum floor heave of the monitored section was 4 cm, so no additional prevention measures are required.

4.2.2 Roof separation characteristics

(1) Roadway separation at Section II

The monitoring data presented in Fig. 14 demonstrates that: (1) When the working face is approximately 15 m ahead it begins to exhibit separation of layers. As the working face is advanced this increases gradually. (2) As the separation increases, the deep base point increases significantly, with a maximum of 12 mm recorded. The shallow base point is maintained at approximately 4 mm, indicating that the separation occurs below this point. (3) The total amount of separation is small, which indicates that the bolt mesh support is effective and the roof separation is controlled.

2) Roadway separation at Section III

The monitoring results presented in Fig. 15 show that; (1) In general, the roof separation of measuring point No.2 gradually increases with the advance of the working face. There is generally separation approximately 25 m ahead of the working face, and the maximum value is about 10 mm. (2) When the working face is advanced within 10 meters, the amount of separation increases. (3) The total amount of separation is small, indicating that the bolt mesh support effect is effective and the roof separation is controlled.

4.2.3 Stress analysis of anchor and cable

The stress trend of anchor rod and anchor cable is shown in Fig. 16.

Analysis of the monitoring data shows that; (1) With the advance of the working face, the stress on the bolt increases. The maximum stress of bolt dynamometer in Section II and

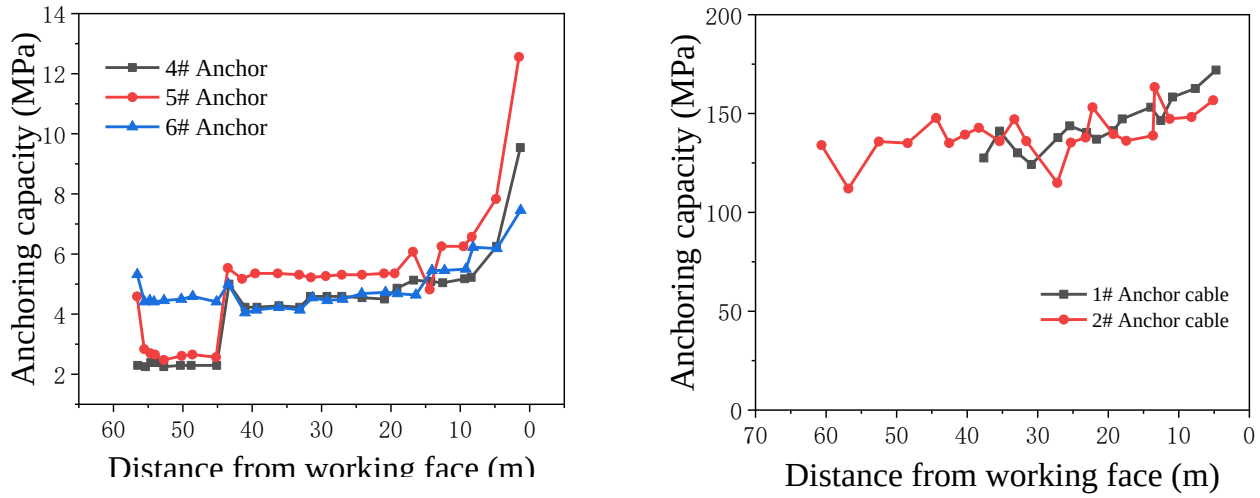

(a) Rock bolt stress change (b) Anchor cable stress change

Fig. 16 Rock bolt and anchor cable stress change

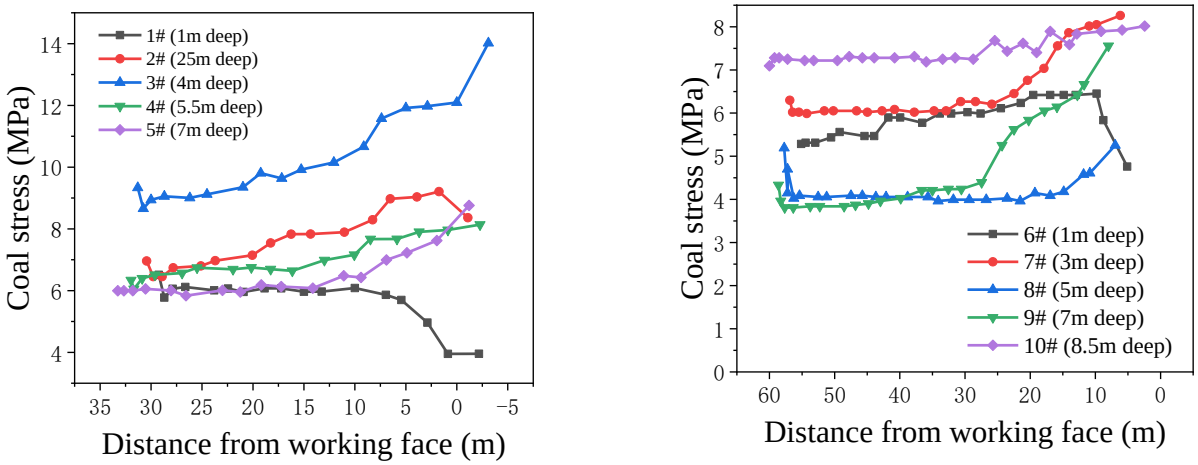

Fig. 17 Change curve of coal stress with working face advancing

III is 5 MPa and 12.5 MPa, respectively. The range affected by advance mining is 12 m~ 15 m in front of the coal wall. (2) With the advancement of the working face, the stress on the anchor cable in Section II and III increases. The maximum stress of anchor cable dynamometer in Section II and III is 172 KN and 156 KN, respectively. The range of influence of advance mining on the anchor cable is 15 m in front of coal wall.

Analysis of the roadway roof separation and anchor cable stress demonstrated that the support of the return air roadway is sufficient and the occurrence of surrounding rock separation is effectively controlled by both the bolt and anchor cable.

4.2.2 Stress distribution law of coal body and isolation wall

The change of stress in coal body is shown in Fig. 17.

Fig. 17 demonstrates that: (1) When the 1# and 2# boreholes are 5 m ahead of the working face, the stress gradually decreases as the coal body is relatively close to the free face (coal wall) of the roadway. (2) The stress of each borehole is relatively stable when beyond 30 m of the advancing working face. However, it changes within 25 m indicating that the stress of the 30 m coal body is the maximum range affected by mining activity. (3) The stress of the 6# borehole decreases sharply when it is approximately 10 m away from the working face. This indicates that the coal mass (1 m deep) in this area has suffered plastic damage. The two groups of borehole stress data show that the stress of each borehole decreased in the initial stage of installation. This is likely due to the initial stress of the installed meter being greater than the actual coal stress. Over time the stress meter gradually equilibrated to the actual coal stress. The coal body on the free face (coal wall) inward to 1.0 m~ 3 m depth will eventually be crushed and plastic failure will occur. The distance where by mining of the working face will have an influence is approximately 25 m.

According to the stress change at the isolation wall 1# measuring point (Fig. 18), the maximum compressive stress is about 5.5 MPa. This roof pressure is not enough to

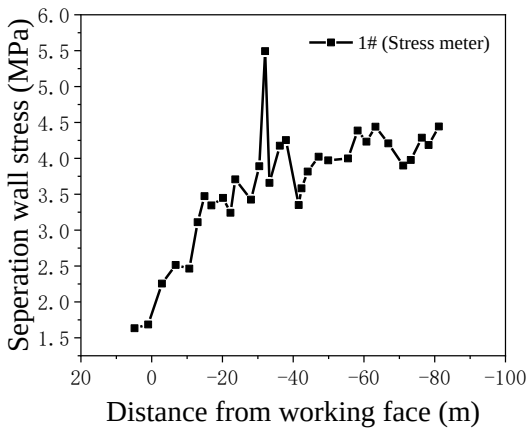

Fig. 18 Curve of separation wall stress at the measuring point 1#

destroy the isolation wall. It still is elastic and has the ability to support the overlying rock mass. After 60 m of mining, the stress inside the isolation wall is maintained at approximately 4 MPa, which is in good agreement with the theoretical calculation. At 20-60 m behind the working face, the internal pressure stress of the isolation wall is 2-6 Mpa, which is consistent with the violent roof movement at this position. As it is close to the working face, the internal stress of the isolation wall changes under the roof weighting. Past 60 m behind the working face, the influence of roof weighting becomes negligible and the wall stress is relatively stable.

5 Conclusions

Through theoretical analysis, laboratory tests, on-site monitoring and other research methods, this study systematically analyzed the use of a double lane roadway with a pre-set isolation wall. This was tested in an outburst prone mine roadway of the Anshun coal mine, The key findings are as follows:

(1) The mechanical model of the broken basic roof is established. The isolation wall is protected by the roadway support when constructed. During the mining process, a part of the basic roof is retained, which is different from the side entry support along the gob side. However, its movement characteristics are similar to that of gob side entry retaining.

(2) Based on the height width ratio of roadside support in gob side entry retaining test, and taking into consideration the stability of the isolation wall, the width is taken as 1 m, the bearing capacity of the isolation wall is 4.66 MN/m, the deformation of the separation wall is approximately 25 cm and the actual settlement should be smaller than the calculation would indicate.

(3) In order to reduce the difficulty of support, the roadway is driven by 5 m. After the construction of the separation wall is completed, the left side coal wall is brushed 1.5 m to make the width of gas roadway 2.5 m. The roadway support consisted of "bolt + ladder beam + anchor cable beam + net". During construction, the concrete pump and removable self-propelled hydraulic wall mold are used to pump and pour the concrete of the isolation wall.

(4) During the process of mining, the total deformation of surrounding rock of roadway and the amount of roof separation in the roadway is small. The stress of the bolt and anchor cable is within the breaking force demonstrating adequate strength as a support system. The required support to the roadway is achieved.

The pre-installed isolation wall in the lane into a double lane without coal pillar protection solution can alleviate the mine mining succession relationship, alleviate the gas overrun phenomenon that often occurs during the digging process, facilitate gas extraction, improve the coal recovery rate, help to cope with stress concentration and coal pillar spontaneous combustion and other safety problems, and consume less manpower and material resources, low production costs. And the overall support effect of the roadway is better; the isolation wall is less stressed and the strength meets the requirements. This solution has a reference role for gas control in mines with similar conditions and can be vigorously promoted in high gas mines.

Acknowledgements

This work is supported by the National Natural Science Foundation of China (52104204), Taishan Scholars Project, Taishan Scholar Talent Team Support Plan for Advantaged & Unique Discipline Areas, Natural Science Foundation of Chongqing, China (cstc2019jcyj-bsh0041), Postdoctoral Science Foundation Project Funded by State Key Laboratory of Coal Mine Disaster Dynamics and Control (2011DA105287-BH201903), Natural Science Foundation of Shandong Province (ZR202103050647) and Natural Science Foundation of Hebei Province (E2019508100). We thank anonymous reviewers for their comments and suggestions to improve the manuscripts.

References

Bai, Q.S., Tu, S.H. and Zhang, C. (2016), "Discrete element modeling of progressive failure in a wide coal roadway from water-rich roofs", *Int. J. Coal Geology*, **167**, 215-229. https://doi.org/10.1016/j.coal.2016.10.010.

Brunschwiler, T., Madhour, Y. and Tick, T. (2013), "Investigation of novel solder patterns for power delivery and heat removal support", *Electronic Components & Technology Conference*, *IEEE*. https://doi.org/10.1109/ECTC.2013.6575605.

Chen, K., Song, M. and Wei, W. (2018), "Structure optimization of parallel air-cooled battery thermal management system with U-type flow for cooling efficiency improvement", *Energy*, **145**(2), 603-613. https://doi.org/10.1016/j.energy.2017.12.110.

Cheng, S., Ma, Z. and Gong, P. (2020), "Controlling the deformation of a small coal pillar retaining roadway by non-penetrating directional pre-splitting blasting with a deep hole: A case study in Wangzhuang coal mine", *Energies*, **13**(12), 3084. https://doi.org/10.3390/en13123084.

Diller, David, E. and Shuck, T. (2015), "Estimation and interpretation of high-confidence microseismic source mechanisms", *Leading Edge*, **34.8**, 918-924.

https://doi.org/10.1190/tle34080918.1.
Feng, J.J., Wang, E.Y. and Huang, Q.S. (2020), "Study on coal fractography under dynamic impact loading based on multifractal method", *Fractals*, **28**(1), 2050006. https://doi.org/10.1142/S0218348X20500061.
Guo, W., Wang, H. and Chen, S. (2016), "Coal pillar safety and surface deformation characteristics of wide strip pillar mining in deep mine", *Arabian J. Geosci.*, **9**(2), 1-9. https://doi.org/10.1007/s12517-015-2233-5.
Hu, S.B., Pang, S.G. and Yan, Z.Y. (2019), "A new dynamic fracturing method: deflagration fracturing technology with carbon dioxide", *Int. J. Fracture*, **220**(1), 99-111. https://doi.org/10.1007/s10704-019-00403-8.
Kong, X.G., Wang, E.Y. and Li, S.G. (2019), "Dynamic mechanical characteristics and fracture mechanism of gas-bearing coal based on SHPB experiments", *Theor. Appl. Fract. Mech.*, **105**, 102395. https://doi.org/10.1016/j.tafmec.2019.102395.
Li, X.L., Cao, Z.Y. and Xu, Y.L. (2020), "Characteristics and trends of coal mine safety development", *Energy Sources, Part A: Recovery, Utilization, and Environmental Effects*, 1-14. https://doi.org/10.1080/15567036.2020.1852339.
Li, X.L., Chen, S.J. and Li, Z.H. (2021), "Rockburst mechanism in coal rock with structural surface and the microseismic (MS) and electromagnetic radiation (EMR) response", *Eng. Fail. Anal.*, **124**(6), 105396. https://doi.org/10.1016/j.engfailanal.2021.105396.
Li, X.L., Chen, S.J. and Liu, S.M. (2021), "AE waveform characteristics of rock mass under uniaxial loading based on Hilbert-Huang transform", *J. Central South Univ.*, **28**(6), 1843-1856. https://doi.org/10.1007/s11771-021-4734-6.
Li, X.L., Chen, S.J. and Zhang, Q.M. (2021), "Research on theory, simulation and measurement of stress behavior under regenerated roof condition", *Geomech. Eng.*, **26**(1), 49-61. https://doi.org/10.12989/gae.2021.26.1.049.
Liu, S.M., Li, X.L. and Wang, D.K. (2021), "Experimental study on temperature response of different ranks of coal to liquid nitrogen soaking", *Nat. Resour. Res.*, **32**(2), 1467-1480. https://doi.org/10.1007/s11053-020-09768-3.
Lobanova, T., Lindin, G. and Trofimova, O. (2017), "Rock mass diagnostics based on microseismic monitoring data at sheregesh deposit", *Proceedings of the IOP Conference Series Earth and Environmental ence*, **53**, 012006. https://doi.org/10.1088/1755-1315/53/1/012006.
Mahdi, A., Shakibaeinia, A. and Dibike, Y.B. (2020), "Numerical modelling of oil-sands tailings dam breach runout and overland flow", *The Science of the Total Environment*, **703**(PT.2),134568.1-134568.10. https://doi.org/10.1016/j.scitotenv.2019.134568
Mcclung, R.C. (2010), "Crack closure and plastic zone sizes in fatigue. Fatigue & Fracture of Engineering", *Mater. Struct.*, **14**(4), 455-468. https://doi.org/10.1111/j.1460-2695.1991.tb00674.x.
Najafi, M., Jalali, S.E. and Bafghi, A.R.Y. (2011), "Prediction of the confidence interval for stability analysis of chain pillars in coal mines", *Saf. Sci.*, **49**(5), 651-657. https://doi.org/10.1016/j.ssci.2010.11.005.
Pokharel, F.M. (2010), "Coupled effects of sulphate and temperature on the strength development of cemented tailings backfills: Portland cement-paste backfill", *Cement Concrete Compos.*, **32**(10), 819-828. https://doi.org/10.1016/j.cemconcomp.2010.08.002.
Qin, Y., Liang, J. and Huang, Z. (2016), "Painting the roadway embankment with non-white high reflective pigments to raise the albedo", *Environ. Earth Sci.*, **75**(4), 1-7. https://doi.org/10.1007/s12665-016-5273-6.
Rezaei M., Hossaini, M.F. and Majdi, A. (2015), "Determination of Longwall Mining-Induced Stress Using the Strain Energy Method", *Rock Mech. Rock Eng.*, **48**(6), 2421-2433. https://doi.org/10.1007/s00603-014-0704-8.
Rezagholilou, A., Nikraz, H. and Green, P.P. (2015), "Effects of nano-silica on cement-fly ash modified crushed rocks base materials", **2**(1), 1-6. https://doi.org/10.15436/2377-1372.15.007.
Sander, R. and Connell, L.D. (2012), "Methodology for the economic assessment of enhanced coal mine methane drainage (ECMM) as a fugitive emissions reduction strategy", *International J. Greenhouse Gas Control*, **8**, 34–44. https://doi.org/10.1016/j.ijggc.2012.01.009.,
Shen, W.L., Wang, M. and Cao, Z.Z. (2019), "Mining-induced failure criteria of interactional hard roof structures: A case study", *Energies*, **12**, 3016:1-17. https://doi.org/10.3390/en12153016.
Singh, R., Mandal, P.K. and Singh, A.K. (2011), "Coal pillar extraction at deep cover: With special reference to Indian coalfields", *Int. J. Coal Geology*, **86**(2-3), 276-288. https://doi.org/10.1016/j.coal.2011.03.003
Singh, R., Singh, A.K. and Maiti, J. (2011), "An observational approach for assessment of dynamic loading during underground coal pillar extraction", *Int. J. Rock Mech. Min.ences*, **48**(5), 794-804. https://doi.org/10.1016/j.ijrmms.2011.04.003.
Soares, C.G. and Cherneva, Z. (2005), "Spectrogram analysis of the time–frequency characteristics of ocean wind waves", *Ocean Eng.*, 2005, **32**(14-15), 1643-1663. https://doi.org/10.1109 / ECTC.2013.6575605.
Song, Z. (2015), "A new method to improve operating performance for underground hard rock mining with new scheduling, controlling and forecasting techniques", *IEEE T. Magn.*, **33**(5), 4113-4115. https://doi.org/10.1109/20.619680.
Tinnea, R., Tinnea, J. and Kuder, K. (2016), "High-early-strength, high-resistivity concrete for direct-current light rail", *J. Mater. Civil Eng.*, **29**(4), 04016260. https://doi.org/10.1061/(ASCE)MT.1943-5533.0001812.
Tiskumara, R., Joshi, R.P. and Mauch, D. (2015), "Analysis of high field effects on the steady-state current-voltage response of semi-insulating 4h-sic for photoconductive switch applications", *J. Appl. Phys.*, **118**(9), 1732-G193. https://doi.org/10.1063/1.4929809.
Vladimir, M. Anastasia, M. and Shevtsov, B. (2017), "Application of sensor signal analysis network complex for distributed, time synchronized analysis of electromagnetic radiation", *E3s Web of Conferences*, **20**, 02010. https://doi.org/ 10.1051/e3sconf/20172002010.
Wang, C., Song, D.Z., Zhang, C.L., Liu, L., Zhou, Z.H. and Huang, X.C. (2019), "Research on the classification model of coal's bursting liability based on database with large samples", *Arabian J. Geosci.*, **12**(13), 411 https://doi.org/10.1007/s12517-019-4562-2.
Wang, Q., Feng, J.J. and Yan, P.Y. (2011), "An explanation for the negative effect of elevated temperature at early ages on the late-age strength of concrete", *J. Mater. Sci.*, **46**(22), 7279-7288. https://doi.org/10.1007/s10853-011-5689-z.
Wang, S.F., Li, X.B. and Yao, J. (2019), "Experimental investigation of rock breakage by a conical pick and its application to non-explosive mechanized mining in deep hard rock", *Int. J. Rock Mech. Min. Sci.*, **122**, 104063. https://doi.org/10.1016/j.ijrmms.2019.104063.
Wang, X., Bai, J. and Wang, R. (2015), "Bearing characteristics of coal pillars based on modified limit equilibrium theory", *Int. J. Min. Sci. Technol.*, **25**(6), 943-947. https://doi.org/10.1016/j.ijmst.2015.09.010.
Wang, X., Yuan, W. and Yan, Y. (2020b), "Scale effect of mechanical properties of jointed rock mass: A numerical study

based on particle flow code", *Geomech. Eng.*, **21**(3), 259-268. https://doi.org/10.12989/gae.2020.21.3.259.

Wohlford, A., Ravindran, S. and Kidane, A. (2019), "Energy absorption characteristics of graded foams subjected to high velocity loading: Proceedings of the 2018 annual conference on experimental and applied mechanics", *Dynam. Behavior of Mater.*, **1**, 229-232. https://doi.org/10.1007/978-3-319-95089-1_41.

Wu, N., Liang, Z.Z. and Zhou, J.R. (2020), "Energy evolution characteristics of coal specimens with preformed holes under uniaxial compression", *Geomech. Eng.*, **20**(1), 55-66. https://doi.org/10.12989/gae.2020.20.1.055.

Yan, H., Zhang, J.X. and Li, L.Y. (2018), "Prediction of upper limit position of bedding separation overlying a coal roadway within an extra-thick coal seam", *J. Central South Univ.*, **25**(2), 448-460. https://doi.org/10.1007/s11771-018-3749-0.

Yang, X.L., Wen, G.C. and Dai, L.C. (2019), "Ground subsidence and surface cracks evolution from shallow-buried close-distance multi-seam mining: A case study in Bulianta coal mine", *Rock Mech. Rock Eng.*, **52**(8), 2835-2852. https://doi.org/10.1007/s00603-018-1726-4.

Zhang, C.L., Xu, J. and Yin, G.Z. (2019), "A novel large-scale multifunctional apparatus to study the disaster dynamics and gas flow mechanism in coal mines", *Rock Mech. Rock Eng.*, **52**(2), 2889-2898. https://doi.org/10.1007/s00603-018-1610-2.

Zhang, Z.B., Wang, E.Y., Liu, X.N., Zhang, Y., Li, S., Khan, M. and Gao, Y. (2021), "Anisotropic characteristics of ultrasonic transmission velocities and stress inversion during uniaxial compression process", *J. Appl. Geophys*., **186**, 104274. https://doi.org/10.1016/j.jappgeo.2021.104274.

Zhang, R., Liu, J. and Sa, Z.Y. (2020), "Fractal characteristics of acoustic emission of gas-bearing coal subjected to true triaxial loading", *Measurement*, https://doi.org/10.1016/j.measurement.2020.108349.

Zhu, G.L., Sousa, R.L. and He, M.C. (2020), "Stability analysis of a non-pillar-mining approach using a combination of discrete fracture network and discrete-element method modeling", *Rock Mech. Rock Eng.*, **53**(1), 269-289. https://doi.org/10.1007/s00603-019-01901-w.

Zhang, X., He, M. and Yang, J. (2020), "An innovative non-pillar coal-mining technology with automatically formed entry: A case study", *Engineering,* https://doi.org/10.1016/j.eng.2020.01.014.

Zhou, C., Jiang, F. and Xu, D. (2020), "A calculation model to predict the impact stress field and depth of plastic deformation zone of additive manufactured parts in the process of ultrasonic impact treatment", *J. Mater. Process. Technol.*, **280,** 116599. https://doi.org/10.1016/j.jmatprotec.2020.116599.

Zou, Q., Liu, H. and Cheng, Z. (2020), "Effect of slot inclination angle and borehole-slot ratio on mechanical property of pre-cracked coal: Implications for ECBM recovery using hydraulic slotting", *Nat. Resour. Res.*, **29**(3), 1705-1729. https://doi.org/10.1007/s11053-019-09544-y.